

See discussions, stats, and author profiles for this publication at: <https://www.researchgate.net/publication/268217711>

In Situ Preparation of Highly Stable Ni-Based Supported Catalysts by Solution Combustion Synthesis

ARTICLE *in* THE JOURNAL OF PHYSICAL CHEMISTRY C · NOVEMBER 2014

Impact Factor: 4.77 · DOI: 10.1021/jp508546n

CITATIONS

4

READS

106

8 AUTHORS, INCLUDING:



[Khachatur V. Manukyan](#)

University of Notre Dame

61 PUBLICATIONS 256 CITATIONS

[SEE PROFILE](#)



[A. S. Rogachev](#)

Institute of Structural Macrokinetics and Mate...

131 PUBLICATIONS 1,351 CITATIONS

[SEE PROFILE](#)



[D. Yu. Kovalev](#)

Institute of Structural Macrokinetics and Mate...

59 PUBLICATIONS 312 CITATIONS

[SEE PROFILE](#)



[Eduardo E. Wolf](#)

University of Notre Dame

119 PUBLICATIONS 3,976 CITATIONS

[SEE PROFILE](#)

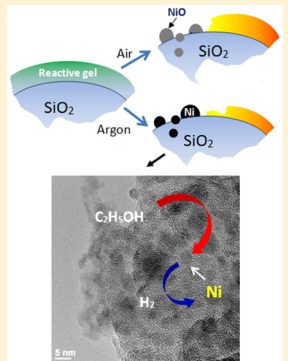
In Situ Preparation of Highly Stable Ni-Based Supported Catalysts by Solution Combustion Synthesis

Allison Cross,[†] Sergey Roslyakov,[‡] Khachatur V. Manukyan,[§] Sergei Rouvimov,^{||} Alexander S. Rogachev,[‡] Dmitry Kovalev,[‡] Eduardo E. Wolf,[†] and Alexander S. Mukasyan^{*,†}

Departments of [†]Chemical and Biomolecular Engineering, [§]Physics, and ^{||}Electrical Engineering, University of Notre Dame, Notre Dame, Indiana 46556, United States

[‡]Center of Functional Nano-Ceramics, National University of Science and Technology, "MISIS", Moscow, 119049, Russia

ABSTRACT: Solution combustion synthesis (SCS) is typically used to produce nanostructured oxides and bulk metallic materials for a variety of application including catalysis. Here, we report in situ, one-step SCS of high surface area ($155 \text{ m}^2/\text{g}$) Ni catalysts supported on fumed silica (SiO_2). Time-resolved X-ray diffraction is used to investigate the dynamics of phase formation during combustion of nickel nitrate–glycine–ammonium nitrate reactive gels impregnated onto porous SiO_2 . It is shown that highly dispersed nickel nanoparticles (5 nm) formed in the reaction front are followed by their rapid oxidation by air oxygen. To prevent the undesired oxidation process, the synthesis was conducted in an inert atmosphere (argon, helium). It is demonstrated that low concentration oxygen impurity (less than 0.001 wt %) in the inert gas passivates the Ni nanoparticles through the formation of a thin amorphous oxide layer. The thus prepared Ni/SiO_2 supported catalyst possesses high activity during the ethanol decomposition toward hydrogen at low temperatures (200°C) and excellent stability toward deactivation with essentially no change of catalyst activity over 100 h of operation.



1. INTRODUCTION

Nickel-based catalysts are active and selective for a range of chemical reactions such as those occurring in petroleum refining including hydro-treating,^{1,2} hydro-cracking,^{2,3} and hydro-processing.^{4,5} Nickel-based catalysts are also used for hydrogen production from ethanol (decomposition,^{6–8} steam reforming,^{9–14} and oxidative steam reforming^{15,16}). Ethanol is nontoxic, easily transported through the current infrastructure, and is considered as a potential hydrogen generation source. The stability of catalysts, however, is the most important challenge in all pathways for hydrogen production from ethanol. Recently, deactivation aspects of catalysts during ethanol conversion were thoroughly reviewed.¹⁷ Catalyst deactivation is generally attributed to the deposition of carbonaceous species, as well as the sintering and oxidation of metallic particles.

Various approaches are reported for the synthesis of Ni-supported catalysts, including incipient wetness,¹⁸ impregnation,^{19,20} coprecipitation,^{20–22} and sol–gel^{23,24} methods, which produce catalysts with a high specific surface area. Nickel nitrates^{23,25} are often used as a precursor throughout these preparation techniques, although nickel hydroxides²⁶ and acetates^{27,28} can also be used. For example, for the hydrogenation of benzene, the nickel catalyst is derived from nickel acetate precursors.^{29,30} Nickel acetate is also the precursor for a nickel-based catalyst used for catalyzing the methane reforming process, which is highly important for the production of hydrogen. However, these synthesis methods typically require an additional heat treatment (calcination) to obtain the desired phase composition, which could lead to significant sintering.

Solution combustion synthesis (SCS) is another viable method for catalyst preparation. SCS is typically a redox based reaction that takes place in a homogeneous aqueous solution of oxidizing (e.g., metal nitrates) and reducing agents (fuels).^{31–33} Glycine is one of the most popular reducing agents as it readily dissolves in water and forms complexes with metal nitrates.³⁴ These mixtures react exothermically after ignition, generating high-energy output, which is sufficient to produce crystalline materials in a single self-sustained step. This form of combustion offers some unique features for material synthesis. The reaction is completed within a short time (on the order of seconds) with maximum temperatures as high as $\sim 1500^\circ\text{C}$. Such high temperatures facilitate formation of crystalline material and usually no calcination is required to obtain the desired phase composition. More importantly, the mixing of precursors on the molecular level and release of large quantities of gases, such as carbon dioxide, water, and nitrogen, result in the formation of nanoscaled solid porous products.

SCS is used to prepare nanosized materials for various applications, including bulk and supported catalysts.^{6,7,34–45} Specifically, solution combustion synthesis is used for the preparation of oxide-based catalysts with a surface area higher than those obtained by coprecipitation methods.^{31–34} Recently, several transition metals (Ni, Cu, Fe) and alloys (Cu–Fe–Ni) have also been synthesized by this method.^{35–38,42,46,47} It is shown that the combustion of nickel (and/or copper) nitrate +

Received: August 23, 2014

Revised: October 14, 2014

Published: October 17, 2014

glycine mixture at near-stoichiometric and fuel-lean conditions produces fine oxide powders. However, excessive quantities of fuel lead to the formation of pure metal (e.g., Ni, Cu) or alloy (Ni–Cu–Fe). SCS is also used to produce supported catalysts as a porous support can further improve the dispersion of the active phase and enhance the structural and thermal stability of the catalysts. Indeed, an inert support used in SCS facilities formation of smaller and dispersed particles. However, regardless of fuel to oxidizer ratio, the final supported catalysts always involve only oxide phases.^{7,34,40,41,48,49}

In this work, we report SCS of silica supported active metal (nickel) catalysts in an argon atmosphere. The thus prepared Ni/SiO₂ supported catalyst possesses high activity during ethanol decomposition to produce hydrogen at low temperatures (200 °C) and it has excellent stability toward deactivation with essentially no change of catalyst activity over 100 h of operation.

2. MATERIAL AND METHODS

To prepare Ni/SiO₂ catalysts reactive solutions containing nickel nitrate hydrate (Ni(NO₃)₂·6H₂O, Alfa Aesar, 98%), ammonium nitrate (NH₄NO₃, Alfa Aesar, 98%), and glycine (C₂H₅NO₂, Alfa Aesar, 98.5%) with different fuel to oxidizer (nickel nitrate) ratios (φ) were dissolved in 6 g of deionized water and thoroughly stirred. The quantities of used reactants are summarized in Table 1.

Table 1. Quantities of Reactants Used in Preparation of Reactive Solutions

fuel/oxidizer ratios (φ)	reactant (g)		
	Ni(NO ₃) ₂ ·6H ₂ O	C ₂ H ₅ NO ₂	NH ₄ NO ₃
1.25	3.89	1.4	1.4
3	3.89	3.36	1.81

The amount of ammonium nitrate added was 20 wt % of the total weight of the solid reactive mixture. This addition over the stoichiometry is required to maintain high combustion temperature and allow the combustion front to self-propagate throughout the porous media of the inert silica support. The reactive mixture was dissolved in water (6 g) and the obtained aqueous solution was then impregnated onto 2 g of fumed silica (Alfa Aesar, surface area of ~400 m²/g) in three increments. First, 6 g of solution was added to the silica, well mixed, and then dried at 70 °C for 2 h. This process was repeated two more times but with the addition of 1.5 g of the solution each time. The dried material was then pressed into a 30 mm diameter pellet and placed in a reactor with a gas feed under different gas atmospheres (air or argon) and pressures (0.1–1 MPa). The purity of argon was 99.993% with oxygen content less than 0.001%, which, although low, has an important role in the results obtained. The reaction was initiated by the local preheating (spot of ~1 mm³) of the pellet by a resistively heated tungsten wire. After ignition, the chemical reaction propagated through the sample in the form of a rapidly moving combustion wave. Samples reacted in argon were left in the reactor for 15 min to cool down to room temperature.

The temperature–time profile of the process was recorded by 100 μm K-type thermocouples inserted inside the pellet. The output signal of the thermocouple was collected by a data acquisition system (Data Translation Inc.) and recorded with 1 kHz frequency using Quick DAC software. The velocity of the

combustion wave propagation was calculated from data obtained from different thermocouples located at known distances along the direction of the reaction front.

Time-resolved XRD (TRXRD) was used for in situ monitoring of the dynamics of phase transformation in the reaction front. The experimental procedure for TRXRD studies can be found elsewhere.^{50,51} The reactive sample was placed into the reaction chamber and then a tungsten wire was used for local reaction initiation at one end of the sample. In one selected experiment, helium (99.995% pure) was used as an inert gas to investigate the behavior of the Ni formed during the synthesis process. The TRXRD system, including a CuKα X-ray source, monochromator, and a linear position-sensitive detector is used to obtain a wide range (2θ up to 25–75°) of diffraction spectra with a time resolution of 10 patterns per second. The crystallinity and phase composition of the catalysts were determined by standard X-ray diffraction (XRD) analysis with Ni-filtered Cu Kα radiation (D8 Advance, Bruker) operated at 40 kV and 40 mA. Step-scan size of 0.025° and counting time of 1 s were recorded for the angular range of 30–90° (2θ).

X-ray photoelectron spectroscopy (XPS) measurements were carried out in a PHI VersaProbe II spectrometer with an Al Kα X-ray source operating at 1486.6 eV and a 90° takeoff angle for near surface analysis of C 1s and Ni 2p3 electronic transitions. Catalyst powders were adhered to stainless steel mounts and loaded into the analysis chamber. Samples were outgassed in the vacuum system maintained at a pressure less than ~10⁻⁷ Pa. Binding energy values were referenced to the C 1s peak (284.8 eV) that resulted from the adventitious contamination layer. The spectra were analyzed using the Multipak XPS software package.

Scanning (SEM) and transmission electron microscopy (TEM) were used to characterize the composition and morphology of the catalysts, as well as their atomic structure. The microstructural analysis was conducted in a FESEM Magellan 400 (FEI), with a resolution of 0.6 nm, which is also equipped with an energy dispersive X-ray spectrometer (EDS, Bruker) with an energy resolution of 123 eV. A Titan 80–300 HRTEM (FEI) with resolution of 0.136 nm in STEM mode and about 0.1 nm information limit in HRTEM mode, was also used. The Titan is equipped with an energy dispersive X-ray spectroscopy (EDS, Oxford Inc.) system with a spectral energy resolution of 130 eV.

The specific surface area of the products was measured by the BET method using an ASAP 2020 instrument (Micromeritics). Prior to this analysis, the samples were vacuum degassed at 100 °C for 15 h. Catalytic activity and selectivity during ethanol decomposition were measured in a continuous flow fixed bed quartz reactor at atmospheric pressure as described elsewhere.^{6,7} The supported catalysts with ~20 wt % of Ni loading were ground into a fine powder, pressed into a wafer, grounded again, and then sieved to select particles from 0.6 to 1 mm in size to limit effects of diffusion. 0.4 g of the catalyst was placed into the reactor and reduced with hydrogen at 300 °C for 1 h. After purging with nitrogen for several hours, the nitrogen was then passed through a bubbler filled with ethanol and sent to the reactor, operating at temperatures varying from room temperature to up to 400 °C. The products in the reactor effluent were analyzed using two gas chromatographs connected in parallel to measure the resulting gas concentrations. Conversion and product selectivity were calculated as described in Eqs 1–3,⁵² where n_i is the molar

flow rate and ν_i is the ratio of the stoichiometric factors between the carbon containing products and ethanol:

$$X_{\text{EtOH}} = \frac{n_{\text{EtOH,in}} - n_{\text{EtOH,out}}}{n_{\text{EtOH,in}}} \times 100 \quad (1)$$

$$\chi_i = \frac{n_i}{\nu_i n_{\text{EtOH,in}}} \quad (2)$$

$$\chi_{H_2} = \frac{n_{H_2}}{3n_{\text{EtOH,in}}} \quad (3)$$

3. RESULTS AND DISCUSSION

The $\text{Ni}(\text{NO}_3)_2$ –glycine– NH_4NO_3 reactive mixtures impregnated onto fumed silica were used to prepare supported Ni/SiO₂ catalysts via the SCS method, varying the fuel to oxidizer ratio (φ) as well as the atmosphere (air, argon, helium) in the reaction chamber at gas pressures (P) in the range of 0.1–0.5 MPa.

3.1. Synthesis of Ni-SiO₂ Catalysts. It was shown previously that the combustion of nickel nitrate–glycine mixtures in air results in the formation of NiO for reactive solutions with φ ratio below 1.25.^{35,53} This result is expected from the stoichiometry, since NiO is a product of nickel nitrate decomposition at temperatures equal to those observed in the combustion wave. More interestingly, we found that pure Ni can be formed as the only solid product at higher fuel to oxidizer ratios ($\varphi \geq 1.25$).⁵³ Recently, we reported the nontrivial reaction mechanism of metal formation in the combustion wave.³⁵ In situ studies revealed that ammonia (NH₃) formed in the self-sustained reaction front reduces nickel oxide to pure metal and rapid ($\sim 100^\circ\text{C}/\text{s}$) natural cooling of the product prevents its consecutive oxidation in air.

It was expected that a similar mechanism would also work during the combustion reaction in nickel nitrate–glycine solution impregnated on the porous high surface area silica support. However, our experiments indicate that on the supported catalyst, regardless of the φ value, which was varied in the range of 1–3, the only detected combustion product was the NiO phase (Figure 1, curves a and b). TRXRD experiments, which allow us to monitor the evolution of phase formation in the reaction front with a 1 s time span

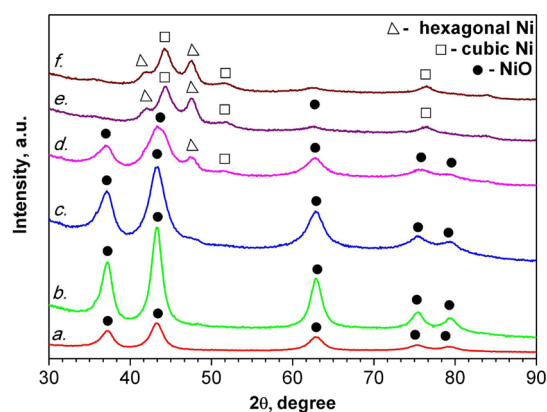


Figure 1. Results of XRD analysis of combustion products of $\text{Ni}(\text{NO}_3)_2$ + glycine + NH_4NO_3 + SiO_2 mixtures at different atmospheres and pressures: (a) $\varphi = 1.25$ in air 0.1 MPa, (b) $\varphi = 3$ in air, 0.1 MPa, (c) $\varphi = 3$ in Ar 0.1 MPa, (d) $\varphi = 3$ in Ar, 0.2 MPa, (e) $\varphi = 3$ in Ar, 0.3 MPa, (f) $\varphi = 3$ in Ar, 0.5 MPa.

(Figure 2A) provide an explanation to this result. It can be seen that initially the reactive media is amorphous ($t = 25$ s). During

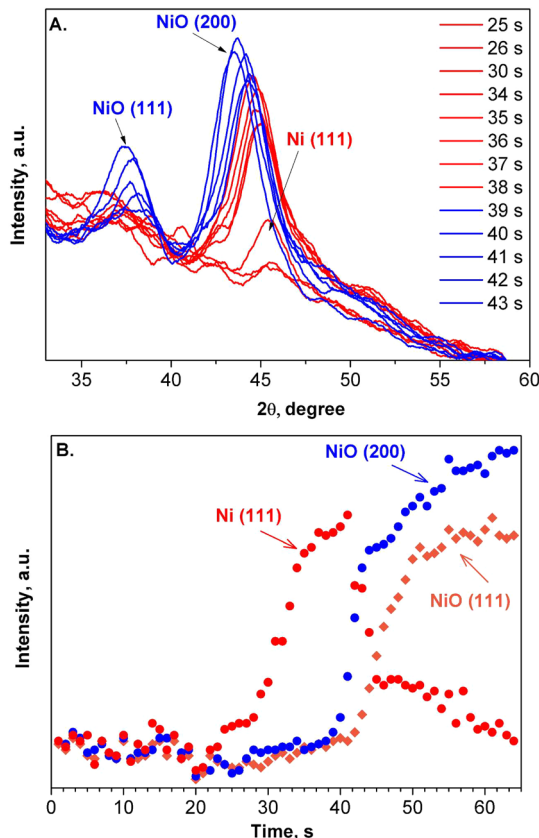


Figure 2. Sequence of TRXRD patterns (A) and kinetics of phase formation (B) during combustion of $\text{Ni}(\text{NO}_3)_2$ + glycine + NH_4NO_3 + SiO_2 mixture ($\varphi = 3$) in air, $P = 0.1$ MPa.

the first reaction stage, when the combustion front is passing along the investigated region of the sample ($t = 27$ –35 s) only Ni(111) can be detected. During the second reaction stage, in the postcombustion zone ($t > 35$ s), the relative intensity of Ni peak decreases, while NiO peaks appear and grow. The corresponding kinetics of phase transformation, that is, peak intensity as a function of time, is shown in Figure 2B. Taking into account that the velocity of the combustion front propagation is 1 mm/s and the width of the investigated area is ~ 2 mm, it can be concluded that NiO peaks emerge 5–7 s after the reaction front passed through the area.

As mentioned above, the reoxidation of nickel does not take place during combustion of unsupported samples, made from nickel nitrate–glycine gels ($\phi > 1.25$). The reason for this effect can be found from the analysis of the microstructure of the products (Figure 3). Nickel formed during the combustion of a nickel nitrate–glycine solution has foam-like microstructure and micron size scale of heterogeneity (Figure 3A). The product formed during the combustion of the impregnated media has a highly porous nanoparticulate structure with particle size of ~ 5 nm. (Figure 3B). Therefore, the extremely fine Ni particles formed in the combustion front oxidize even during the relatively short duration (~ 10 s) of the postcombustion.

One way to overcome oxidation is to conduct experiments in an inert atmosphere. Such experiments may also address the issue of the influence of the air-oxygen on the combustion wave

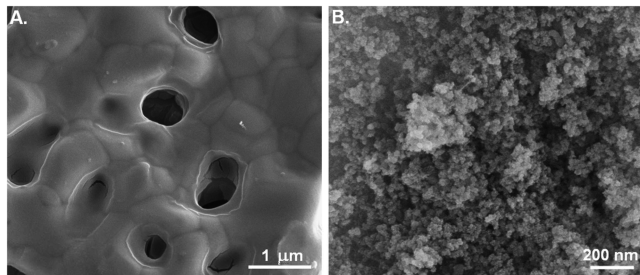


Figure 3. Microstructures of combustion product for $\text{Ni}(\text{NO}_3)_2 + \text{glycine}$, $\varphi = 1.25$ gel (A) and $\text{Ni}(\text{NO}_3)_2 + \text{glycine} + \text{NH}_4\text{NO}_3 + \text{SiO}_2$ mixture, $\varphi = 3$.

propagation in such systems. Typical time–temperature profiles for the combustion wave propagation along the silica impregnated by the reactive solution are shown in Figure 4 A–C. It can be seen that the maximum combustion temperature essentially does not depend on the Ar pressure (P_{Ar}) in the reactor, being on the order of 700 °C. The velocity of the combustion wave increases with increase of P_{Ar} (Figure 4D). This effect can be related to the fact that higher gas pressure in the reactor leads to less expansion of the media in the reaction front, including SiO_2 support, providing higher thermal conductivity of the porous media resulting in an increase of reaction front propagation velocity.⁵⁴ The values of the maximum combustion temperature and velocity of the reaction front propagation obtained in argon and air are similar. However, oxidation of nickel formed in the postcombustion

zone could be seen on the time–temperature profile of the sample reacted in air (Figure 4B, curve b.). These results confirm the conclusions that air–oxygen does not influence the reaction in the combustion front but oxidizes nickel later in the postcombustion zone.

TRXRD data obtained in an inert atmosphere (helium) further demonstrates (Figure 5) that only a Ni phase is formed in the combustion front. However, XRD analysis of the final products obtained in argon at 0.1 and 0.2 MPa contain only NiO phase (Figure 1, curves c and d). Complete conversion of nickel nitrate to Ni could be observed only at 0.5 MPa of argon pressure (Figure 1, curve f). These results appear inconsistent and do not have a trivial explanation. On the one hand, it appears that the oxidation of extremely fine (5 nm) Ni particles takes place when they are exposed to air after synthesis and complete cooling. The temperature of the product increases again when the reactor is opened and the product is exposed to the atmosphere. On the other hand, the absence of NiO peaks after synthesis at higher ($P > 0.4$ MPa) argon pressure needs further investigation as it appears that a small amount of oxygen impurities (less than 0.001 wt %) in argon at some critical gas pressure becomes sufficient to passivate the surface of ultrafine Ni particles with a thin amorphous layer of NiO phase. Being amorphous, this NiO layer is not detectable by XRD even after exposure to the air for 2–3 days. The presence of a surface NiO layer is confirmed by the XPS results of the catalyst (Figure 6) prepared at 0.5 MPa of Ar. The Ni 2p^{3/2} spectra show the

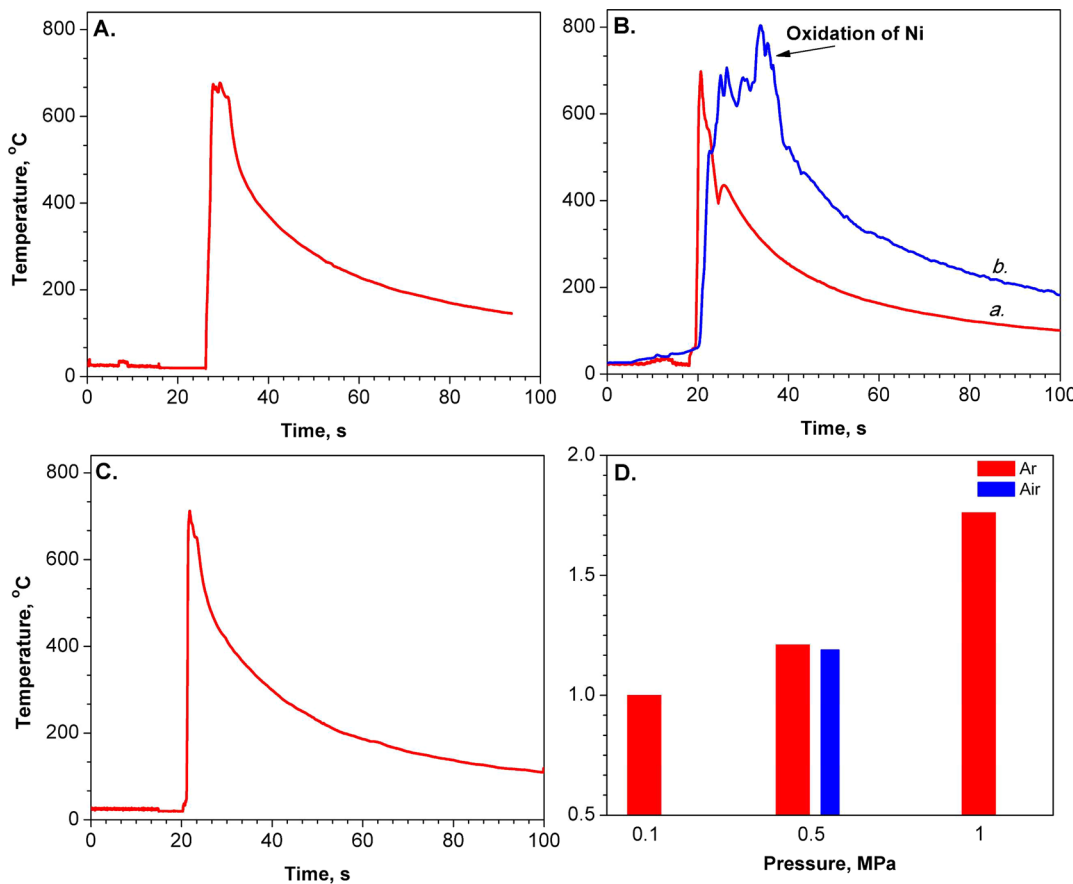


Figure 4. Temperature–time profiles (A–C) and combustion front propagation velocities (D) of $\text{Ni}(\text{NO}_3)_2 + \text{glycine} + \text{NH}_4\text{NO}_3 + \text{SiO}_2$ mixtures with $\varphi = 3$: (A) 0.1 MPa Ar, (B) 0.5 MPa Ar (curve a) and air (curve b), and (C) 1 MPa Ar pressures.

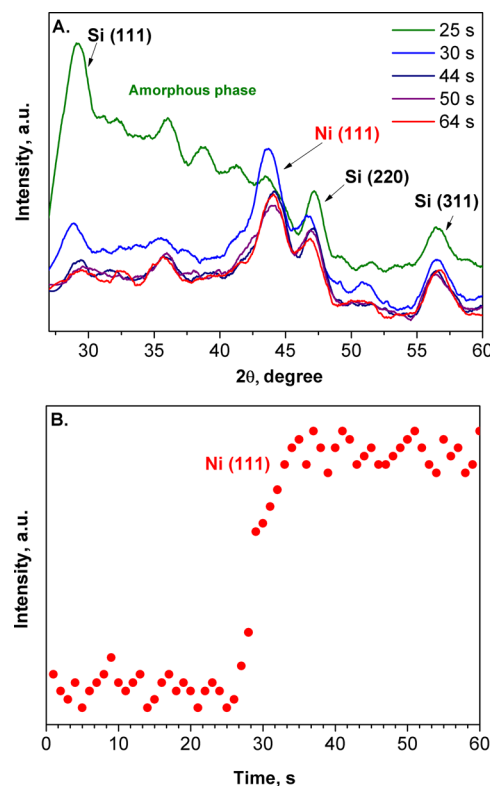


Figure 5. Sequence of TRXRD patterns (A) and kinetics of phase formation (B) during combustion of $\text{Ni}(\text{NO}_3)_2$ + glycine + NH_4NO_3 + SiO_2 mixture ($\varphi = 3$) in helium, $P = 0.1 \text{ MPa}$ (Si particles were used as a reference point).

presence of both Ni(II) and Ni(0) states at 856 and 852.7 eV energies, respectively.

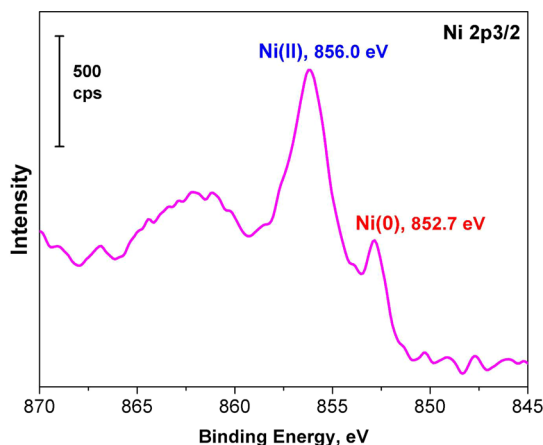


Figure 6. XPS spectrum of Ni for the catalysts prepared at 0.5 MPa of Ar.

XRD results also indicate that the catalysts synthesized at high argon pressure ($P_{\text{Ar}} \geq 0.3 \text{ MPa}$) contain both the stable face-centered cubic (fcc) and metastable hexagonal close-packed (hcp) Ni phases (Figure 1, curve f). It is worth noting that only the fcc phase was observed previously after SCS in air of support-free gels of the same compositions.^{35,36,53} Early reports show that a high temperature is necessary to produce hcp-Ni.^{55,56} It also has been suggested that a high temperature ramp is required to obtain this metastable phase. Both these

conditions are satisfied in the reaction environment of the combustion synthesis processes.

The TEM results also agree well with the above interpretation of the formation of a passivation layer at high P_{Ar} . Figure 7A shows a typical bright-field TEM image of the catalysts resulted from SCS reaction at 0.5 MPa of argon pressure ($\varphi = 3$). The material consists of porous agglomerates that contain amorphous silica and nanosized Ni crystals. The diffraction pattern inserted in Figure 7A confirms that Ni particles are crystalline. The HRTEM images (Figure 7B,C) of the agglomerate in the catalyst provide evidence that the Ni nanoparticles are approximately 2–5 nm in diameter and are embedded in the highly porous SiO_2 matrix (one can note crystalline particles surrounded by an amorphous matrix). The lattice fringes that are seen in Figure 7C correspond to Ni crystalline lattice. A HAADF STEM image of the product shown in Figure 8A confirms these observations. Indeed, the STEM contrast (so-called Z-contrast) depends on atomic weight: and the contrast in Figure 8A is brighter for heavier atoms (Ni) and darker for lighter elements (Si and O). EDS spectra confirms that the bright contrast is associated with Ni (Figure 8B), while the gray contrast is sole silica (Figure 8C). The agglomerate in Figure 8A is supported by a lacey carbon film so that the imaged area is under vacuum (no overlapping with carbon supporting film). Thus, EDS spectra do not contain any substantial amount of carbon signal. The atomic ratio $[\text{Si}]/[\text{O}]$ is close to 1:2, which is typical for silica. In the case of the EDS spectrum of Figure 8B, all three elements, Ni, Si, and O, are present because Ni particles are embedded in the silica matrix. Thus, both STEM image and EDS spectra show evidence of a high dispersion of small Ni particles onto the high surface area silica. The BET specific surface area of Ni-SiO_2 synthesized at 0.5 MPa of argon is $155 \text{ m}^2/\text{g}$, which confirms the TEM data that SCS allows fabrication of supported catalysts with highly dispersed metal nanoparticles.

3.2. Catalytic Activity and Selectivity. The SCS Ni-SiO_2 catalyst with highly dispersed nickel particles is a good candidate for ethanol decomposition to hydrogen. The typical data of conversion and selectivity of methane, carbon monoxide, hydrogen, and acetaldehyde during ethanol decomposition over one of the Ni/SiO_2 catalysts are shown in Figure 9. It can be seen that 90% conversion of ethanol with hydrogen selectivity of ~30% can be reached at relatively low temperature (200°C). The comparison of data on ethanol conversion and hydrogen selectivity over Ni/SiO_2 and unsupported Ni catalysts (Figure 10) demonstrates that the former one possesses much higher activity and selectivity than the latter, in the investigated temperature range.

Figure 11 displays the activity and selectivity results of the ethanol decomposition reaction to H_2 , CH_4 , and CO over 100 h time on stream (TOS) at 200°C . Throughout the reaction, ethanol is converted over 90%, and the selectivity values for methane, carbon monoxide, and hydrogen are ~40, 37, and 30%, respectively, which indicate essentially full ethanol decomposition, with a small fraction of acetaldehyde being produced. It can be seen that the catalyst showed no decrease in activity or selectivity during 100 h. Note that the same bulk unsupported Ni catalysts (prepared by SCS) deactivated within several hours of the start of reaction (Figure 11). Therefore, the high dispersion of the nickel particles is crucial in developing a highly active and selective catalyst for stable hydrogen production.

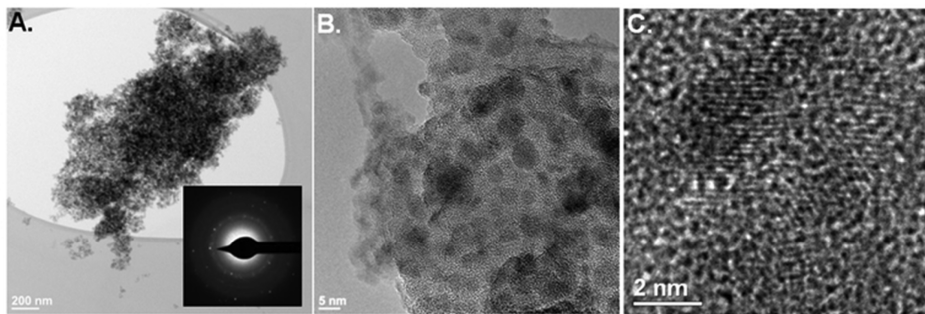


Figure 7. TEM/HRTEM images of Ni/SiO₂ catalyst prepared at 0.5 MPa pressure of argon: low (A) and high (B and C) magnifications. Diffraction pattern is the inset in (A).

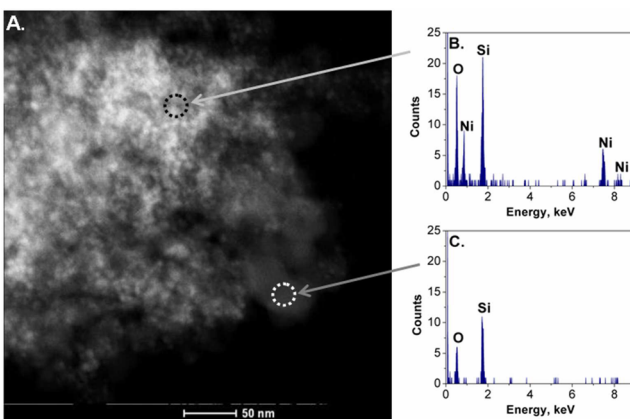


Figure 8. STEM image (A) and EDX spectra (B,C) of Ni/SiO₂ catalysts prepared at 0.5 MPa pressure of argon.

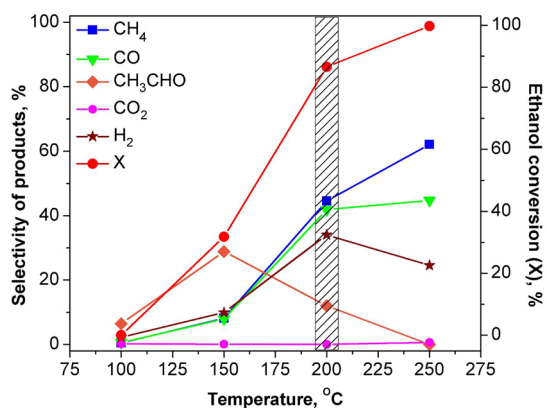


Figure 9. Typical data on conversion (X) and selectivity of methane, carbon oxides, hydrogen, and acetaldehyde during the ethanol decomposition over Ni/SiO₂ catalysts.

The surface composition of the catalyst was studied with XPS over the as-synthesized sample (Figure 12, curve a) and after the 100 h reaction (Figure 12, curve b). The carbon-related peak at \sim 285 eV shows no change after 100 h of reaction and corresponds to \sim 7.0% surface carbon. This is an important result as formation of carbonaceous species is a major issue in ethanol reforming reactions, leading to the rapid deactivation of the catalyst. Moreover, the specific surface area of the spent catalyst (after 100 h) was exactly the same ($155\text{ m}^2/\text{g}$) as before the reaction. Those data indicate that the SCS supported Ni/SiO₂ is an excellent candidate for long-term production of hydrogen from ethanol.

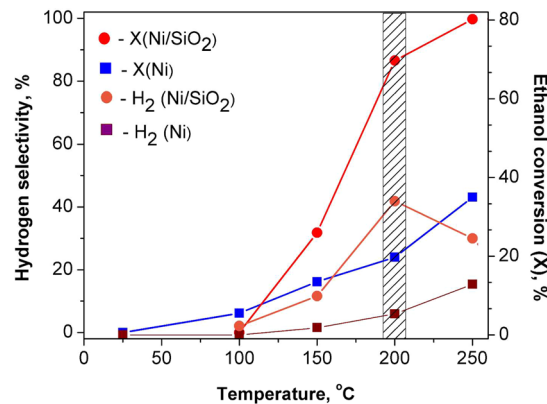


Figure 10. Conversion and selectivity of ethanol decomposition over Ni/SiO₂ and unsupported Ni catalysts.

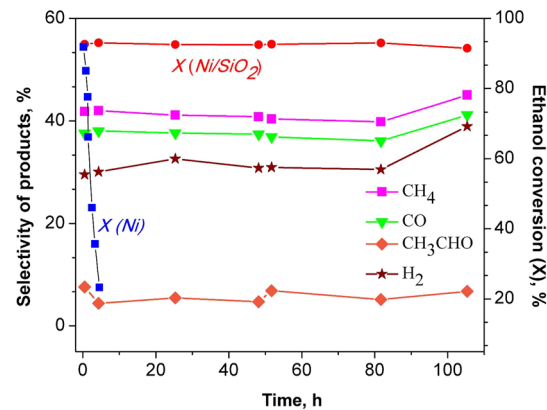


Figure 11. Conversion ($X(\text{Ni})$) over unsupported Ni catalysts, conversion ($X(\text{Ni/SiO}_2)$) and selectivity of methane, carbon monoxide, hydrogen, and acetaldehyde during the ethanol decomposition over Ni/SiO₂ catalyst, 200 °C.

4. CONCLUSION

Solution combustion synthesis was used to prepare only oxide based materials until recently when bulk metals could be produced. However, adding an inert support to the combustion process allows the formation of dispersed oxide active material on supported oxides. Here, we demonstrate that under an inert gas at slightly higher than ambient pressure produces passivated ultrasmall Ni nanoparticle dispersed on silica during a combustion process. Combustion synthesized Ni/SiO₂ catalysts show high activity and excellent stability toward deactivation

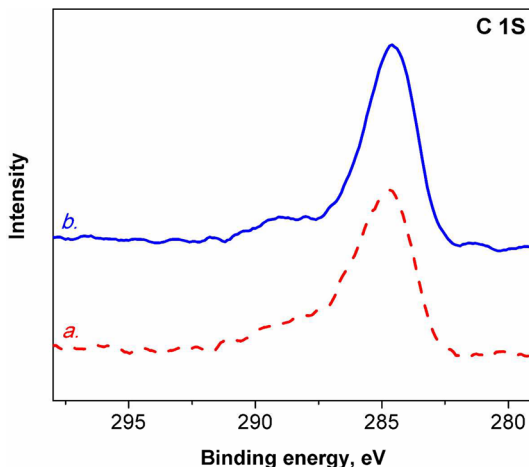


Figure 12. Results of XPS analysis of combustion synthesized Ni/SiO₂ catalysts prepared at 0.5 MPa pressure of argon (curve a) and after 100 h TOS of ethanol decomposition (curve b).

during the ethanol decomposition reaction at low temperatures over 100 h with no change in the catalyst.

AUTHOR INFORMATION

Corresponding Author

*E-mail: amoukasi@nd.edu. Phone: 574-631-9825.

Notes

The authors declare no competing financial interest.

ACKNOWLEDGMENTS

This work was supported by the Ministry of Education and Science and Education of the Russian Federation in the framework of Increase Competitiveness Program of NUST “MISIS” Grant No. K2-2014-001. We thank the Center for Sustainable Energy at Notre Dame (cSEND) Materials Characterization Facilities. We acknowledge support of the National Science Foundation through MRI Award 1126374 for the XPS data in this paper. We would also like to thank the Notre Dame Integrated Imaging Facility (NDIIF) for use of their imaging equipment.

REFERENCES

- Zhang, X.; Wang, T.; Ma, L.; Zhang, Q.; Jiang, T. Hydrotreatment of Bio-Oil over Ni-Based Catalyst. *Bioresour. Technol.* **2013**, *127*, 306–311.
- Tiwari, R.; Rana, B. S.; Kumar, R.; Verma, D.; Kumar, R.; Joshi, R. K.; Garg, M. O.; Sinha, A. K. Hydrotreating and Hydrocracking Catalysts for Processing of Waste Soya-Oil and Refinery-Oil Mixtures. *Catal. Commun.* **2011**, *12*, 559–562.
- Grilec, M.; Likozar, B.; Levec, J. Hydrodeoxygenation and Hydrocracking of Solvolysed Lignocellulosic Biomass by Oxide, Reduced and Sulphide Form of NiMo, Ni, Mo, and Pd Catalysts. *Appl. Catal., B* **2014**, *150–151*, 275–287.
- Veriansyah, B.; Han, J. Y.; Kim, S. K.; Hong, S.; Kim, Y. J.; Lim, J. S.; Shu, Y.; Oh, S.; Kim, J. Production of Renewable Diesel by Hydroprocessing of Soybean Oil: Effect of Catalysts. *Fuel* **2012**, *94*, 578–585.
- Zhao, H. Y.; Li, D.; Bui, P.; Oyama, S. T. Hydrodeoxygenation of Guaiacol as Model Compound for Pyrolysis Oil on Transition Metal Phosphide Hydroprocessing Catalysts. *Appl. Catal., A* **2011**, *391*, 305–310.
- Kumar, A.; Mukasyan, A. S.; Wolf, E. E. Combustion Synthesis of Ni, Fe and Cu Multi-Component Catalysts for Hydrogen Production from Ethanol Reforming. *Appl. Catal., A* **2011**, *401*, 20–28.
- Cross, A.; Kumar, A.; Wolf, E. E.; Mukasyan, A. S. Combustion Synthesis of a Nickel Supported Catalyst: Effect of Metal Distribution on the Activity During Ethanol Decomposition. *Ind. Eng. Chem. Res.* **2012**, *51*, 12004–12008.
- Akdim, O.; Cai, W.; Fierro, V.; Provendier, H.; van Veen, A.; Shen, W.; Mirodatos, C. Oxidative Steam Reforming of Ethanol Over Ni-Cu/SiO₂, Rh/Al₂O₃ and Ir/CeO₂: Effect of Metal and Support on Reaction Mechanism. *Top. Catal.* **2008**, *52*, 22–38.
- Wang, W.; Wang, Y. Steam Reforming of Ethanol to Hydrogen over Nickel Metal Catalysts. *Int. J. Energy Res.* **2010**, *34*, 1285–1290.
- Fatsikostas, A. N.; Verykios, X. E. Reaction Network of Steam Reforming of Ethanol over Ni-Based Catalysts. *J. Catal.* **2004**, *225*, 439–452.
- Rossetti, I.; Biffi, C.; Bianchi, C. L.; Nicelle, V.; Signoretto, M.; Menegazzo, F.; Finocchio, E.; Ramis, G.; Michele, A. D. Ni/SiO₂ and Ni/ZrO₂ Catalysts for the Steam Reforming of Ethanol. *Appl. Catal., B* **2012**, *117–118*, 384–396.
- Sanchez-Sanchez, M. C.; Navarro, R. M.; Kondarides, D. I.; Verykios, X. E.; Fierro, J. L.G. Mechanistic Aspects of the Ethanol Steam Reforming Reaction for Hydrogen Production on Pt, Ni, and PtNi Catalysts Supported on γ -Al₂O₃. *J. Phys. Chem. A* **2010**, *114*, 3873–3882.
- Haryanto, A.; Fernando, S.; Murali, N.; Adhikari, S. Current Status of Hydrogen Production Techniques by Steam Reforming of Ethanol: A Review. *Energy Fuels* **2005**, *19*, 2098–2106.
- Xu, W.; Liu, Z.; Johnston-Peck, A. C.; Senanayake, S. D.; Zhou, G.; Stacchiola, D.; Stach, E. A.; Rodriguez, J. A. Steam Reforming of Ethanol on Ni/CeO₂: Reaction Pathway and Interaction between Ni and the CeO₂ Support. *ACS Catal.* **2013**, *3*, 975–984.
- Deluga, G. A.; Salge, J. R.; Schmidt, L. D.; Verykios, X. E. Renewable Hydrogen from Ethanol by Autothermal Reforming. *Science* **2004**, *303*, 993–997.
- de Lima, S. M.; da Silva, A. M.; da Costa, L. O. O.; Assaf, J. M.; Mattos, L. V.; Sarkari, R.; Venugopal, A.; Noronha, F. B. Hydrogen Production Through Oxidative Steam Reforming of Ethanol over Ni-Based Catalysts Derived from La_{1-x}Ce_xNiO₃ Perovskite-Type Oxides. *Appl. Catal., B* **2012**, *121–122*, 1–9.
- Mattos, L. V.; Jacobs, G.; Davis, B. H.; Noronha, F. B. Production of Hydrogen from Ethanol: Review of Reaction Mechanism and Catalyst Deactivation. *Chem. Rev.* **2012**, *112*, 4094–4123.
- Chang, F.; Kuo, M.; Tsay, M.; Hsieh, M. Hydrogenation of CO₂ over Nickel Catalysts on Rice Husk Ash-Alumina Prepared by Incipient Wetness Impregnation. *Appl. Catal., A* **2003**, *247*, 309–320.
- Wang, S.; Lu, G. Q. M. CO₂ Reforming of Methane on Ni Catalysts: Effects of the Support Phase and Preparation Technique. *Appl. Catal., B* **1998**, *16*, 269–277.
- Li, G.; Hu, L.; Hill, J. M. Comparison of Reducibility and Stability of Alumina-Supported Ni Catalysts prepared by Impregnation and Co-Precipitation. *Appl. Catal., A* **2006**, *301*, 16–24.
- Xu, S.; Wang, X. Highly Active and Coking Resistant Ni/CeO₂-ZrO₂ Catalyst for Partial Oxidation of Methane. *Fuel* **2005**, *84*, 563–567.
- Kruissink, E. C.; van Reijen, L. L.; Ross, R. H. Coprecipitated Nickel-Alumina Catalysts for Methanation at High Temperature. Part 1. Chemical Composition and Structure of the Precipitates. *J. Chem. Soc., Faraday Trans.* **1981**, *77*, 649–663.
- Natesakhawat, S.; Oktar, O.; Ozkan, U. S. Effect of Lanthanide Promotion on Catalytic Performance of Sol-Gel Ni/Al₂O₃ Catalysts in Steam Reforming of Propane. *J. Mol. Catal. A: Chem.* **2005**, *241*, 133–146.
- Ueckert, T.; Lamber, R.; Jaeger, N. I.; Schubert, U. Strong Metal Support Interactions in a Ni/SiO₂ Catalyst Prepared via Sol-Gel Synthesis. *Appl. Catal., A* **1997**, *155*, 75–85.
- Alejandre, A.; Medina, F.; Rodriguez, X.; Salagre, P.; Cesteros, Y.; Sueiras, J. E. Cu/Ni/Al Layered Double Hydroxides as Precursors of Catalysts for the Wet air Oxidation of Phenol Aqueous Solutions. *Appl. Catal., B* **2001**, *30*, 195–207.

- (26) van der Lee, M. K.; van Dillen, A. J.; Bitter, J. H.; de Jong, K. P. Deposition Precipitation for the Preparation of Carbon Nanofiber Supported Nickel Catalysts. *J. Am. Chem. Soc.* **2005**, *127*, 13573–13582.
- (27) Boudjahem, A. G.; Monteverdi, S.; Mercy, M.; Bettahar, M. M. Study of Nickel Catalysts Supported on Silica of Low Surface Area and Prepared by Reduction of Nickel Acetate in Aqueous Hydrazine. *J. Catal.* **2004**, *221*, 325–334.
- (28) Li, B.; Watanabe, R.; Maruyama, K.; Kunimori, K.; Tomishige, K. Thermographical observation of Catalyst Bed Temperature in Oxidative Steam Reforming of Methane over Ni Supported on α -Alumina Granules: Effect of Ni Precursors. *Catal. Today.* **2005**, *104*, 7–17.
- (29) Wang, H.; Yu, Z.; Chen, H.; Yang, J.; Deng, J. High Activity Ultrafine Ni-Co-B Amorphous Alloy Powder for the Hydrogenation of Benzene. *Appl. Catal., A* **2005**, *129*, L143–L149.
- (30) Dai, W.; Qiao, M.; Deng, J. XPS Studies on a Novel Amorphous Ni-Co-W-B Alloy Powder. *Appl. Surf. Sci.* **1997**, *120*, 119–124.
- (31) Aruna, S. T.; Mukasyan, A. S. Combustion Synthesis and Nanomaterials. *Curr. Opin. Solid State Mater. Sci.* **2008**, *12*, 44–50.
- (32) Patil, K. C.; Aruna, S. T.; Mimani, T. Combustion Synthesis: An Update. *Curr. Opin. Solid State Mater. Sci.* **2003**, *6*, 507–512.
- (33) Mukasyan, A. S.; Epstein, P.; Dinka, P. Solution Combustion Synthesis of Nanomaterials. *Proc. Combust. Inst.* **2007**, *31*, 1789–1795.
- (34) González-Cortés, S. L.; Imbert, F. E. Fundamentals, Properties and Applications of Solid Catalysts Prepared by Solution Combustion Synthesis (SCS). *Appl. Catal., A* **2013**, *452*, 117–131.
- (35) Manukyan, K. V.; Cross, A.; Roslyakov, S.; Rouvimov, S.; Rogachev, A. S.; Wolf, E. E.; Mukasyan, A. S. Solution Combustion Synthesis of Nano-Crystalline Metallic Materials: Mechanistic Studies. *J. Phys. Chem. C* **2013**, *117*, 24417–24427.
- (36) Kumar, A.; Miller, J. T.; Mukasyan, A. S.; Wolf, E. E. In Situ XAS and FTIR Studies of a Multi-Component Ni/Fe/Cu Catalyst for Hydrogen Production from Ethanol. *Appl. Catal., A* **2013**, *467*, 593–603.
- (37) Kumar, A.; Mukasyan, A. S.; Wolf, E. E. Impregnated Layer Combustion Synthesis Method for Preparation of Multicomponent Catalysts for the Production of Hydrogen from Oxidative Reforming of Methanol. *Appl. Catal., A* **2010**, *372*, 175–183.
- (38) Kumar, A.; Wolf, E. E.; Mukasyan, A. S. Solution Combustion Synthesis of Metal Nanopowders: Copper and Copper/Nickel Alloys. *AIChE J.* **2011**, *57*, 3473–3479.
- (39) Schuyten, S.; Dinka, P.; Mukasyan, A. S.; Wolf, E. A. A Novel Combustion Synthesis Preparation of CuO/ZnO/ZrO₂/Pd for Oxidative Hydrogen Production from Methanol. *Catal. Lett.* **2008**, *121*, 189–198.
- (40) Dinka, P.; Mukasyan, A. S. In situ Preparation of Oxide-Based Supported Catalysts by Solution Combustion Synthesis. *J. Phys. Chem. B* **2005**, *109*, 21627–21633.
- (41) Mukasyan, A. S.; Dinka, P. Novel Approaches to Solution-Combustion Synthesis of Nanomaterials. *Int. J. Self-Propag. High-Temp. Synth.* **2007**, *16*, 23–35.
- (42) Erri, P.; Nader, J.; Varma, A. Controlling Combustion Wave Propagation for Transition Metal/Alloy/Cermet Foam Synthesis. *Adv. Mater.* **2008**, *20*, 1243–1245.
- (43) Deshpande, K.; Mukasyan, A. S.; Varma, A. Direct Synthesis of Iron Oxide Nanopowders by the Combustion Approach: Reaction Mechanism and Properties. *Chem. Mater.* **2004**, *16*, 4896–4904.
- (44) Bhaduri, S.; Bhaduri, S. B.; Zhou, E. Auto Ignition Synthesis and Consolidation of Al₂O₃–ZrO₂ Nano/Nano Composite Powders. *J. Mater. Res.* **1998**, *13*, 156–165.
- (45) Manukyan, K. V.; Chen, Y. S.; Rouvimov, S.; Li, P.; Li, X.; Dong, S.; Liu, X.; Furdyna, J.; Orlov, A.; Bernstein, G. H.; et al. Ultra-Small α -Fe₂O₃ Superparamagnetic Nanoparticles with High Magnetization Prepared by Template-Assisted Combustion Process. *J. Phys. Chem. C* **2014**, *118*, 16264–16271.
- (46) Jung, C. H.; Lee, H. G.; Kim, C. J.; Bhaduri, S. B. Synthesis of Cu–Ni Alloy Powder Directly from Metal Salts Solution. *J. Nanopart. Res.* **2003**, *5*, 383–388.
- (47) Jung, C. H.; Jalota, S.; Bhaduri, S. B. Quantitative Effects of Fuel on the Synthesis of Ni/NiO Particles Using a Microwave-Induced Solution Combustion Synthesis in Air Atmosphere. *Mater. Lett.* **2005**, *59*, 2426–2432.
- (48) Rao, G. R.; Sahu, H. R.; Mishra, B. G. Surface and Catalytic Properties of Cu–Ce–O Composite Oxides Prepared by Combustion Method. *Colloids Surf., A* **2003**, *220*, 261–269.
- (49) Avgouropoulos, G.; Ioannides, T. Selective CO Oxidation over CuO–CeO₂ Catalysts Prepared via the Urea-Nitrate Combustion Method. *Appl. Catal., A* **2003**, *244*, 155–167.
- (50) Khomenko, I. O.; Mukasyan, A. S.; Ponomarev, V. I.; Borovinskaya, I. P.; Merzhanov, A. G. Dynamics of Phase-Forming Processes in Metal-Gas System During Combustion. *Combust. Flame* **1993**, *92*, 201–208.
- (51) Mukasyan, A. S.; White, J. D. E.; Kovalev, D. Y.; Kochetov, N. A.; Ponomarev, V. I.; Son, S. F. Dynamics of Phase Transformation during Thermal Explosion in the Al-Ni System: Influence of Mechanical Activation. *Physica B* **2010**, *405*, 778–784.
- (52) Comas, J.; Marino, F.; Laborde, M.; Amadeo, N. Bio-ethanol Steam Reforming on Ni/Al₂O₃ Catalyst. *Chem. Eng. J.* **2004**, *98*, 61–68.
- (53) Kumar, A.; Wolf, E. E.; Mukasyan, A. S. Solution Combustion Synthesis of Metal Nanopowders. Part 1: Nickel - Reaction Pathways. *AIChE J.* **2011**, *57*, 2207–2214.
- (54) Cano, I. G.; Borovinskaya, I. P.; Rodriguez, M. A.; Grachev, V. V. Effect of Dilution and Porosity on Self-propagating High-temperature Synthesis of Silicon Nitride. *J. Am. Ceram. Soc.* **2002**, *85*, 2209–2211.
- (55) Chen, Y.; Peng, D.; Lin, D.; Luo, X. Preparation and Magnetic properties of Nickel Nanoparticles via the Thermal Decomposition of Nickel Organometallic Precursor in Alkylamines. *Nanotechnology* **2007**, *18*, 505703 (6 pages).
- (56) Mi, Y.; Yuan, D.; Liu, Y.; Zhang, J.; Xiao, Y. Synthesis of Hexagonal Close-packed Nanocrystalline Nickel by a Thermal Reduction Process. *Mater. Chem. Phys.* **2005**, *89*, 359–361.